Nonlinear-optical calculations using fast-transform methods: Second-harmonic generation with depletion and diffraction

Shinan-Chur Sheng and A. E. Siegman
Edward L. Ginzton Laboratory, Stanford, California 94305
(Received 14 September 1979)

The authors describe an analytical approach to nonlinear-optics calculations which is well adapted to obtaining accurate and efficient numerical results for steady-state nonlinear interactions including finite transverse beam profiles, beam-diffraction effects, and power-depletion effects. This general approach is applied to obtain new results for optical second-harmonic generation with both Gaussian and unstable-resonator transverse beam profiles, under large-signal conditions where pump depletion as well as diffraction effects are important.

I. INTRODUCTION

Attempts to obtain accurate numerical results for problems in nonlinear optics and nonlinear optical wave interactions run into severe difficulties as soon as one attempts to include either real optical beam profiles, or optical diffraction effects, or beam-power-depletion effects. Even without these complications, the basic problem is nonlinear. Introducing a finite beam profile increases the dimensionality of the problem; obtaining numerical results for optical diffraction effects is always difficult, even for linear problems; and including power-depletion effects substantially compounds the degree of nonlinearity. Attempting to handle all these aspects at once can seem impracticable. Therefore, previous analyses of nonlinear optics problems have commonly either used infinite-plane-wave approximations, ignoring transverse beam profiles,[1] or have neglected diffraction effects by assuming short interaction lengths,[2] or have neglected beam depletion effects on the grounds that many nonlinear interactions are in practice weak and hence inefficient.[3,4]

On the other hand, there are important practical applications of nonlinear optics—for example, second-harmonic generation of high-power laser beams—which employ real laser beams with sometimes complex transverse profiles,[5] and which lead to energy conversion and pump depletion effects that can be large. One of our objectives in this paper, therefore, is to outline a general formulation for nonlinear wave interaction analyses which includes all of the above effects, and which is also adapted to providing numerical results, employing what we believe to be among the best numerical methods currently available. A second objective is to illustrate the utility of this approach by presenting numerical results for optical second-harmonic generation which include large pump depletion, beam diffraction effects, and real beam profiles including Gaussian beams and unstable-resonator beam profiles.

The essential features of our approach are (i) We extract out the diffraction part of the problem analytically by use of spatial frequency transforms. These transforms are then evaluated numerically using fast-Fourier- or fast-Hankel-transform methods, which are generally believed to be the best approach to numerical analysis of optical diffraction effects. (ii) We solve the resulting reduced differential equations for the nonlinear part of the problem by use of previously developed ordinary-differential-equation (ODE) routines which appear to be well adapted to the problem at hand.

Our approach is still some distance from being universal. In particular it is limited to cw steady-state sinusoidal problems, with no temporal envelope variations or transients. It also assumes a purely macroscopic susceptibility approach to the nonlinear medium, with no provision for transient or "atomic coherence" effects. In addition our approach is primarily intended for more or less parallel and copropagating beams; it would have some difficulty handling problems involving counterpropagating optical beams.

In Sec. II of this paper we outline our basic approach in general terms. Section III applies this approach to the specific case of second-harmonic generation (SHG) using both linearly and cylindrically symmetrical beams. We present numerical results on SHG with strong depletion and diffraction using both Gaussian and unstable-resonator fundamental beam profiles. We also carried out second-harmonic-generation experiments using an unstable-cavity yttrium aluminum garnet (YAG) laser. The experimental data agree well with the numerical results. Section IV finally gives some general discussion of the basic approach and its relative merits and demerits.

II. GENERAL APPROACH

A. Analysis

The starting point for any analysis of nonlinear optical wave interactions is the vector wave equation

$$\nabla^2 \vec{\mathcal{E}}(\vec{r}, z, t) - \mu\epsilon \frac{\partial^2 \vec{\mathcal{E}}(\vec{r}, z, t)}{\partial t^2} = \mu \frac{\partial^2 \vec{\mathcal{P}}_{NL}(\vec{r}, z, t)}{\partial t^2}, \quad (1)$$

where $\vec{r}$ is used as a general form for transverse coordinates written either in Cartesian form $\vec{r} = (x, y)$ or in cylindrical form $\vec{r} = (r, \theta)$. We assume for simplicity of presentation an isotropic but not necessarily dispersionless medium, which means that walk-off effects[3] are not included. This limitation could readily be lifted. The quantities μ and ϵ are to be interpreted as the values appropriate to each frequency component of $\vec{\mathcal{E}}(\vec{r}, z, t)$ separately. The polarization $\vec{\mathcal{P}}_{NL}(\vec{r}, z, t)$ is the nonlinear polarization created in the medium by the total field $\vec{\mathcal{E}}(\vec{r}, z, t)$.

The total field $\vec{\mathcal{E}}(\vec{r}, z, t)$ is then assumed to consist of a set of waves or beams at the various frequencies ω_i traveling more or less along the z axis in the form

$$\vec{\mathcal{E}}(\vec{r}, z, t) = \sum_i \vec{E}_i(\vec{r}, z) e^{j(\omega_i t - k_i z)}, \quad (2)$$

where $k_i^2 \equiv (2\pi/\lambda_i)^2 \equiv \omega_i^2 \mu(\omega_i)\epsilon(\omega_i)$. The complex wave amplitudes $\vec{E}_i(\vec{r}, z, t)$ may be assumed slowly varying in the z direction, i.e., $|\partial^2 \vec{E}_i/\partial z^2| \ll |k_i \partial \vec{E}_i/\partial z|$. By putting the expansion (2) into the wave equation (1) and making the usual paraxial approximation, one may then obtain for each of the waves a separate paraxial equation in the form

$$\frac{\partial \vec{E}_i}{\partial z} = -\frac{j}{2k_i}\nabla_t^2 \vec{E}_i - j\frac{\omega_i \eta_0}{2} e^{jk_i z} \vec{P}_i(\vec{r}, z). \quad (3)$$

Here $\vec{P}_i(\vec{r}, z)$ is that component of the nonlinear polarization having frequency $+\omega_i$ and z variation near to $\exp(-jk_i z)$, and $\eta_0 = (\mu/\epsilon)^{1/2}$. In general, each such component $\vec{P}_i$ will be formed from some nonlinear combination like $\chi_{ijk}\vec{E}_j \vec{E}_k^* \ldots$, with the exact combination depending upon the nature and degree of the specific nonlinearity. A phase mismatch Δk arises if the corresponding vector sum of the wave vectors $\pm k_j \pm k_k \ldots$ is nearly but not exactly matched to k_i.

The first term on the right-hand side of Eq. (3) is the diffraction term for that wave component. We now spatially transform each wave component with respect to its transverse coordinates r in the general form[6]

$$\vec{E}_i(\vec{s}, z) = \int\int \vec{E}_i(\vec{r}, z) K(\vec{s}, \vec{r}) d\vec{r},$$
$$\vec{E}_i(\vec{r}, z) = \int\int \vec{E}_i(\vec{s}, z) K^*(\vec{s}, \vec{r}) d\vec{s}, \quad (4)$$

where $K(\vec{s}, \vec{r})$ means, in general, either the Fourier transform kernel

$$K(\vec{s}, \vec{r}) = \exp[-j2\pi(s_x x + s_y y)], \quad (5a)$$

with $\vec{r} = (x, y), \vec{s} = (s_x, s_y)$, and limits of integration $(-\infty, \infty)$; or else the Hänkel-transform kernel (Fourier-Bessel kernel)

$$K(\vec{s}, \vec{r}) = e^{-il\theta} 2\pi\rho J_l(2\pi\rho r), \quad (5b)$$

with $\vec{r} = (r, \theta), \vec{s} = (\rho, l)$, and limits of integration $(0, \infty)$ for r and $(0, 2\pi)$ for θ. The inverse integral over $d\vec{s}$ in the latter case is actually a continuous integral over $d\rho$ plus a discrete sum over l. From here on we will distinguish the real field amplitudes $\vec{E}_i(\vec{r}, z)$ from their spatial-frequencies transforms $\vec{E}_i(\vec{s}, z)$ by the explicit argument that is indicated.

The diffraction term on the right-hand side of each of Eqs. (3) is then eliminated by transforming each side of the equation and using the substitution

$$\vec{E}_i(\vec{s}, z) = \vec{G}_i(\vec{s}, z)\exp(j\pi\lambda_i s^2 z), \quad (6)$$

where $s^2 = |\vec{s}|^2 = s_x^2 + s_y^2$ for Cartesian coordinates, or $s^2 = \rho^2$ for cylindrical coordinates. The result is

$$\frac{\partial \vec{G}_i(\vec{s}, z)}{\partial z} = -j\frac{\omega_i \eta_0}{2}\exp(-j\pi\lambda_i s^2 z) \times \exp(jk_i z)\int\int \vec{P}_i(\vec{r}, z) K(\vec{s}, \vec{r}) d\vec{s}. \quad (7)$$

This has the form of a large number of coupled ordinary differential equations in z. If we place all the relevant vector components of each $\vec{G}_i$ for all values of i and all values of $\vec{s}$ in a large array G, then the basic equation may be written in symbolic form as

$$\frac{dG}{dz} = F(G, z). \quad (8)$$

Given the transforms $\vec{G}_i(\vec{s}, z)$, at any fixed z one can evaluate the transforms $\vec{E}_i(\vec{s}, z)$ from Eq. (6), the real fields $\vec{E}_i(\vec{r}, z)$ by reverse transformation as in Eq. (4), and the nonlinear polarization $\vec{P}_i(\vec{r}, z)$ from the nonlinear susceptibility tensor of the medium. This then permits evaluation of the derivation array F on the right-hand side of Eq. (8).

Removing the diffraction or beam propagation effects analytically should make the function G in Eq. (8) as slowly varying with z as possible,

since its derivative depends only on the nonlinear interactions. This should then impose in some sense minimum demands upon any numerical routine used to solve Eq. (8). At the same time the Fourier sampling theorem assures that in a numerical calculation the transforms $\vec{E}_i(\vec{s})$ need contain no more information, or no more discrete components, than is needed to describe with sufficient accuracy the field components $\vec{E}_i(\vec{r})$ themselves.

The forward and reverse transforms involved in computing the derivative F are evaluated in practice using either the fast-Fourier-transform (FFT) algorithm,[7-9] or the more recently developed quasi–fast-Hänkel-transform (FHT) algorithm.[10,11] In general the relative speed, accuracy, and storage efficiency of these routines are such as to make them virtually always preferable to other competitive methods for handling complex diffraction problems with the same numerical accuracy. Equation (8) itself is then solved for specified initial conditions by forward integration in z using an optimized ordinary differential equation routine. For this purpose we have employed the set of routines developed by Shampine and Gordon,[12] since this appears to be a carefully tested and highly optimized package.

III. APPLICATION TO SECOND-HARMONIC GENERATION

A. Analysis

In this section we apply the general approach of Sec. II to optical second-harmonic generation. The basic equations for SHG are

$$\nabla_t^2 E_1 - 2jk_1 \frac{\partial E_1}{\partial z} = -2d\omega_1^2\mu_0 E_1^* E_2 e^{-j\Delta kz},$$
$$\nabla_t^2 E_2 - 2jk_2 \frac{\partial E_2}{\partial z} = -d\omega_2^2\mu_0 E_1^2 e^{+j\Delta kz}. \tag{9}$$

The subscripts 1 and 2 refer to the fundamental and second-harmonic waves, respectively; E_1 and E_2 are appropriate scalar E field components of the fundamental and harmonic waves; ∇_t^2 is the Laplacian operator with respect to the transverse coordinates $\vec{r} = (x, y)$ or (r, θ); d is the nonlinearity coefficient for second-harmonic interaction; and $\Delta k = k_2 - 2k_1$ is the k vector mismatch in the nonlinear medium.

It is convenient to normalize the transverse beam coordinates to an arbitrary transverse scale factor w_0 and the E field amplitudes to an arbitrary field E_0. The axial coordinate z may then be scaled to a depletion length z_q or to a diffraction length z_r through the definitions

$$E_1(\vec{r}, z) = E_0 f_1(\vec{r}', l), \quad E_2(\vec{r}, z) = E_0 f_2(\vec{r}', l);$$
$$\vec{r}' \equiv \vec{r}/w_0; \quad l \equiv z/z_q = (z_r/z_q)(z/z_r); \tag{10}$$
$$z_q = \frac{k_1}{\omega_1^2 d\mu_0 E_0} = \frac{2k_2}{\omega_2^2 d\mu_0 E_0}, \quad z_r = \frac{\pi w_0^2}{\lambda_1}.$$

The scaling parameters w_0 and E_0 are basically arbitrary. However, they will be most useful in practice if w_0 is given a value comparable to the fundamental beam radius, and if E_0 is chosen similar to the peak value (or possibly to some cross-section-averaged mean value) of the E field of the fundamental input beam. If, for example, the fundamental beam is a lowest-order Gaussian and w_0 is chosen to be the Gaussian spot size as usual, with E_0 being the peak field strength, then z_r will be the usual Rayleigh range (≡half the confocal parameter) over which diffraction will double the fundamental beam area, and $2^{1/4} z_q$ will be the length at which the second-harmonic power would rise to equal the original input power if both diffraction and depletion were ignored.

The scaled equations are then

$$\frac{\partial f_1}{\partial l} = -\frac{jz_q}{4z_r}\nabla_t'^2 f_1 - j f_1^* f_2 e^{-j\Delta kz_q l},$$
$$\frac{\partial f_2}{\partial z} = -\frac{jz_q}{8z_r}\nabla_t'^2 f_2 - j f_1^2 e^{+j\Delta kz_q l}, \tag{11}$$

where $\nabla_t'^2$ is now the transverse Laplacian with respect to the dimensionless coordinates $\vec{r}' = (x', y')$ or (r', θ). By using the Fourier or Hankel transform pairs,

$$f_i(\vec{r}', l) = \int\int G_i(\vec{s}', l)\exp\left(j\pi^2 \frac{z_q}{z_r} s'^2 l\right) K(\vec{s}', \vec{r}')\, d\vec{r}',$$
$$G_i(\vec{s}', l)\exp\left(j\pi^2 \frac{z_q}{z_r} s'^2 l\right) = \int\int f_i(\vec{r}', l) K^*(\vec{s}', \vec{r}')\, d\vec{s}', \tag{12}$$

where $K(\vec{s}', \vec{r}')$ is the appropriate kernel, the differential equations reduce to

$$\frac{\partial G_1}{\partial l} = -j\exp\left(-j\pi^2 \frac{z_q}{z_r} s'^2 l - j\Delta kz_q l\right)\int\int f_1^* f_2 K^* d\vec{r}',$$
$$\frac{\partial G_2}{\partial l} = -j\exp\left(-j\pi^2 \frac{z_q}{z_r} s'^2 l + j\Delta kz_q l\right)\int\int f_1^2 K^* d\vec{r}'. \tag{13}$$

These equations contain only two independent parameters other than the normalized input functions $f_1(\vec{r}', 0)$ and $f_2(\vec{r}', 0)$: the depletion-to-diffraction-length ratio z_q/z_r, and the depletion–phase-mismatch parameter Δkz_q.

B. Test cases

We programmed Eqs. (13) both in one transverse Cartesian coordinate, i.e., $\vec{r} = x$ and $\vec{s} = s$ only, so that the Fourier transforms reduced to

a one-dimensional FFT, and also in cylindrical coordinates assuming $l=0$ symmetry, so that $\vec{r}=r, \vec{s}=\rho$, and only a radial Hankel transform of order $l=0$ was performed.

In both cases we used the Shampine and Gordon ODE routine[12] for forward integration of Eqs. (13). This routine uses a backward difference Adams-Bashforth algorithm as a predictor of order K, and an Adams-Moulton algorithm as a corrector of order $K+1$, with $K \leq 12$. Typically 512 transverse sampling points were employed, and the local error criterion RELERR in the Shampine and Gordon routine was maintained below 10^{-8}. The calculations were done on an IBM 370/68 computer using the FORTRAN IV-H compiler with OPT =0 using double precision. A typical run for $l=0$–6 took 2 min of CPU time.

The power conversion efficiency for second-harmonic generation is defined as $\eta(z)=P_2(z)/P_1(0)$, where P_1 and P_2 are fundamental and harmonic total beam powers, respectively. For phase-matched uniform plane waves (no diffraction effects) the conversion efficiency is known analytically to be[13]

$$\eta(l)=\tanh^2(l). \tag{14}$$

Setting the parameter $z_q/z_r=0$ in the numerical routine is equivalent to making diffraction effects negligible. We therefore tested the one-dimensional Cartesian FFT routine with a uniform input and zero value of z_q/z_r and found numerical agreement with the $\tanh^2(l)$ function to at least four significant digits at all distances l.

If diffraction effects are in fact negligible, then a transversely nonuniform beam can also be in effect subdivided into many parallel rays or plane-wave sections, to each of which Eq. (14) applies. The conversion efficiency in this case is given by

$$\eta(l)=\frac{\int_{-\infty}^{\infty}\tanh^2[|f_1(x,0)|l]|f_1(x,0)|^2\,dx}{\int_{-\infty}^{\infty}|f_1(x,0)|^2\,dx}. \tag{15}$$

As a test we ran a one-dimensional Gaussian beam of the form $f_1(x,0)=\exp(-x^2)$ with our one-dimensional FFT routine and $z_q/z_r=0$, and again found agreement to the same degree of accuracy.

C. One-dimensional Gaussian beam

As a simple case for gaining physical insight, we calculated the case of a collimated Gaussian fundamental input beam $f_1(x,0)=\exp(-x^2)$ for four different values of $z_q/z_r=0$, 0.5, 1, and 4 assuming the phase-matched condition $\Delta k=0$. The fundamental beam waist is thus at the input plane $z=l=0$. The conversion efficiencies $\eta(l)$ versus distance for these four cases are plotted in Fig. 1.

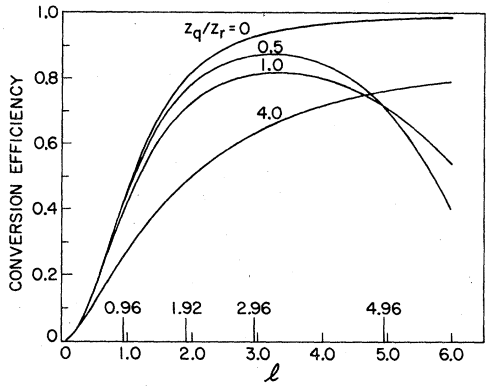

FIG. 1. Conversion efficiency of a one-transverse-dimension Gaussian input wave.

The curve for $z_q/z_r=0$ matches up with Eq. (15). Figure 2 shows the far-field on-axis relative intensities of the fundamental and harmonic versus distance for these same cases.

The curves for finite z_q/z_r exhibit progressively lower conversion efficiencies even at small distances l because the fundamental beam begins to expand owing to diffraction and thus has lower intensity for the same total power. However, the conversion efficiency is also found to turn over at larger l, so that power begins to flow from the harmonic back to the fundamental, at least for $z_q/z_r=0.5$ and 1.0.

To investigate the reason for this turnover, which is unexpected in the nominally phase-

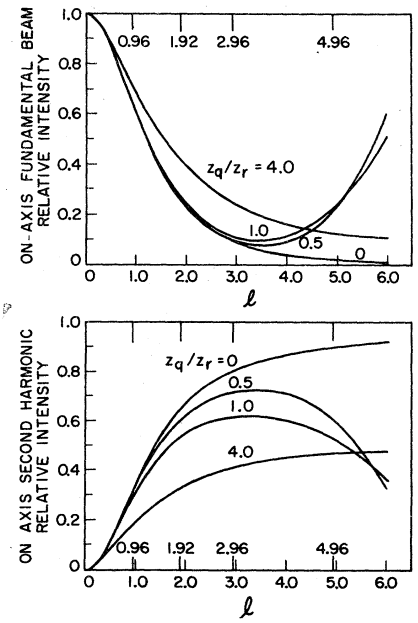

FIG. 2. Far-field on-axis relative intensities of fundamental and second-harmonic waves vs l.

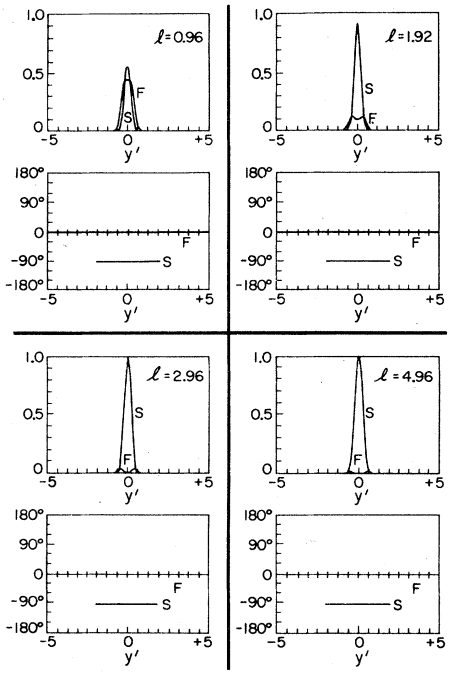

FIG. 3. The intensity profiles (top plot in each block) and phase profiles (lower plot in each block) for $z_q/z_r = 0$ at four different locations, $l = 0.96$, 1.92, 2.96, 4.96.

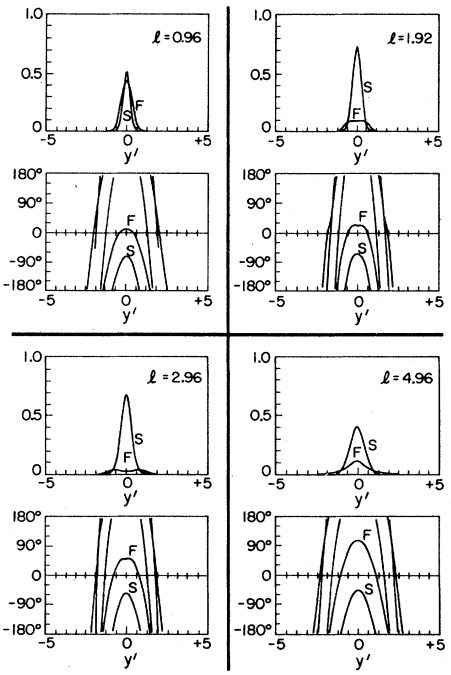

FIG. 4. Same plot as in Fig. 3 with $z_q/z_r = 0.5$.

matched case, we plot both the fundamental and harmonic intensity and phase profiles at four distances $l = 0.96$, 1.92, 2.96, and 4.96 for both $z_q/z_r = 0$ and 0.5 in Figs. 3 and 4. Figure 3 shows that in the no-diffraction case the fundamental beam acquires a depleted hole in the center of the beam, and this hole evenutally expands to consume the entire beam. The phase fronts remain entirely planar with a 90° phase lag between the second-harmonic and fundamental waves.

Figure 4 shows that for the finite-diffraction case the central depletion effect is much reduced. As expected, both the fundamental and harmonic beams have diverging spherical wave fronts. The on-axis phase angle of the fundamental wave rotates slightly forward, in accord with the well-known Guoy effect for Gaussian beams.[14] This phase would approach 90° for $z/z_r \gg 1$. The most important point is that as a result of the complex interplay between harmonic generation and propagation effects, the second-harmonic phase profile shifts forward by a smaller amount. The growth rate for the harmonic function f_2 is given in general terms by

$$\frac{1}{f_2}\frac{df_2}{dl} \propto \left|\frac{f_1^2}{f_2}\right| \exp[j(2\varphi_1 - \varphi_2 - \tfrac{1}{2}\pi)], \qquad (16)$$

where φ_1 and φ_2 are the phase angles of f_1 and f_2, respectively. Between $l = 2.96$ and 4.96, the on-axis value of the net phase angle $(2\varphi_1 - \varphi_2 - \frac{1}{2}\pi)$ moves from a value representing amplitude growth of f_2 to a value representing parametric pumping of energy from the harmonic wave back to the fundamental wave. As illustrated in Fig. 4, the central hole in the fundamental wave fills back in, and significant net power is transferred from the harmonic beam back into the fundamental beam.

This behavior could presumably be modified by using a deliberate phase mismatch, $\Delta k \neq 0$, to compensate for the diffraction phase shifts. However, the optimum value of Δk would be different for each different crystal length and fundamental power level. The parameter space to be explored numerically could thus be very large.

D. Two-dimensional Gaussian beam

Additional results were calculated using the FHT version of this program, with 512 radial points, for a cylindrically symmetric Gaussian beam having a waist located at the center of an SHG crystal of length z_c, as illustrated in Fig. 5. This is the optimum geometry for low input powers. For this case we plot in Fig. 6 the harmonic conversion efficiency through the entire crystal length versus a focusing parameter $z_c/2z_r$, where increasing $z_c/2z_r$ means a more tightly focused waist inside the crystal. The intensity parameter for the individual curves is $K = (z_c z_r/2z_q^2)^{1/2}$, which is directly proportional to

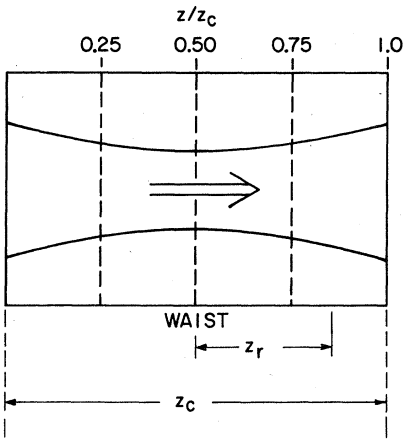

FIG. 5. The configuration of Gaussian-beam symmetrical pumping. z_r is the Rayleigh length; z_c is the crystal length.

the fundamental input power and independent of focusing. As a further check on our routine, the optimum focusing for low input power and $\Delta k = 0$ in our results is observed to be very close to the value $z_c/2z_r \approx \frac{1}{2}\pi$ as predicted by an analytic treatment for the Gaussian beam case ignoring depletion.[15] (Our low-power results do not fall off away from optimum focusing as rapidly as some analytic solutions because we have not included walk-off effects.[3])

For higher input powers, obtaining the optimum conversion efficiency requires progressively weaker focusing ($z_R \gg z_C$). Indeed, if one stays at the optimum focusing value for low input power and simply turns up the input power K, the conversion efficiency rises at first, but then turns around and falls sharply with increasing input, never rising much above 50% efficiency.

To explore this behavior further we plot in Figs. 7 and 8, the beam intensity and phase profiles at four different planes through the crystal, using

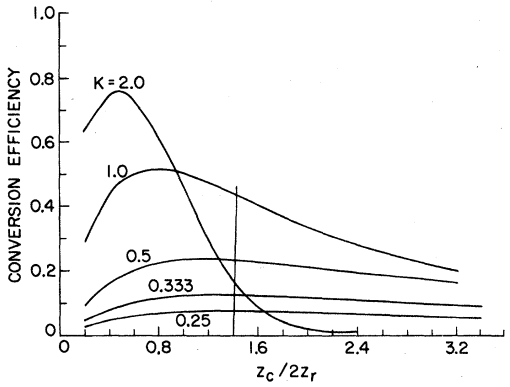

FIG. 6. The conversion efficiencies vs $z_c/2z_r$.

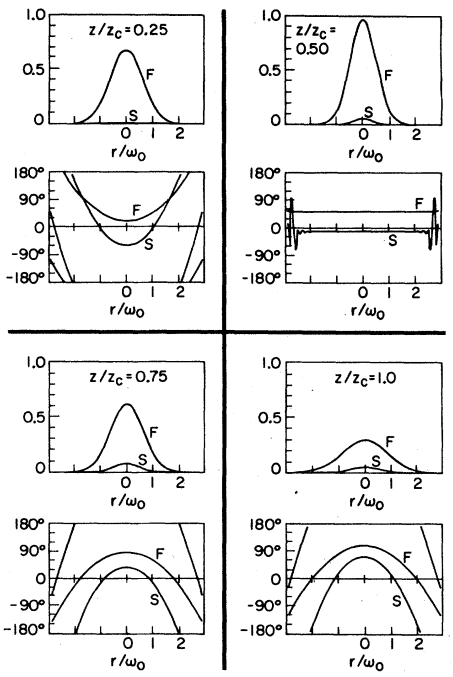

FIG. 7. The intensity profiles (top plot in each block) and phase profiles (lower plot in each block) for normalized input powers $k=0.25$, $z_c/2z_r=1.4$ ($z_a/z_r=4.73$) at four different planes through the crystal.

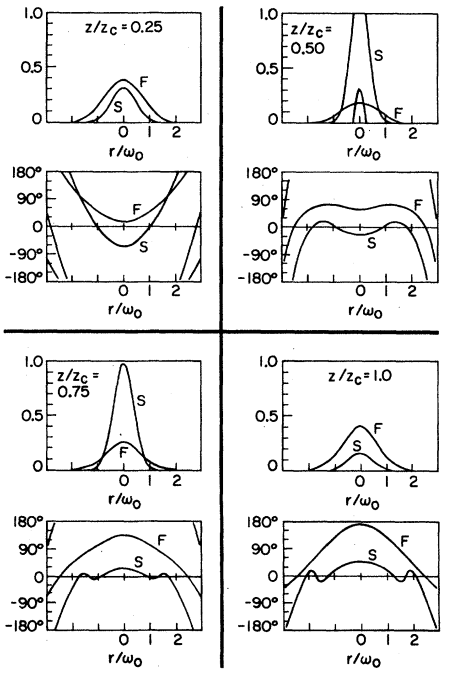

FIG. 8. Same plot as in Fig. 7 for $k=2.0$, $z_c/2z_r=1.4$ ($z_a/z_r=0.59$).

the low-power-optimized focusing, for normalized input powers $K=0.25, z_c/2z_r=1.4(z_q/z_R=4.73)$ and $K=2.0, z_c/2z_r=1.4(z_q/z_r=0.59)$. Again, significant phase variations appear in the higher-power case.

E. Unstable-resonator case

Finally, a separate optical resonator code was used to generate the output beam profile of a confocal unstable laser resonator at $\lambda_1=1.06$ μm with output mirror diameter =0.18 cm, magnification $M=3.5$, and equivalent Fresnel number $N_{eq}=1.5$,[5] and to propagate this beam forward 1 m before reaching the SHG crystal. The fundamental intensity profile shown in Fig. 9 was then used as the input to the cylindrical symmetrical FHT version of the nonlinear code. Figure 10 shows predicted conversion efficiencies versus nonlinear interaction length z/z_q, for different values of z_q/z_r. (This parameter could be adjusted in practice by inserting a telescope to magnify or demagnify the beam diameter.) We may conclude that for sufficiently high powers (small z_q) and large-dimaeter beam (large z_r), an unstable resonator beam can give very high conversion efficiency despite its apparently complex and irregular intensity profile.

Experiments on harmonic generation with an unstable resonator beam were carried out by using a YAG laser with an unstable cavity having the parameters described above. The laser was Q-switched at 10 pulses per second, with an output energy of about 0.5 J per pulse. A 5-cm KD*P crystal was used for Type-I phase matching. Owing to the large laser beam size (≈6 mm) the walk-off effect in the crystal was relatively small and not taken into consideration. The fundamental pulse was roughly Gaussian in time with a width of about 20 nsec.

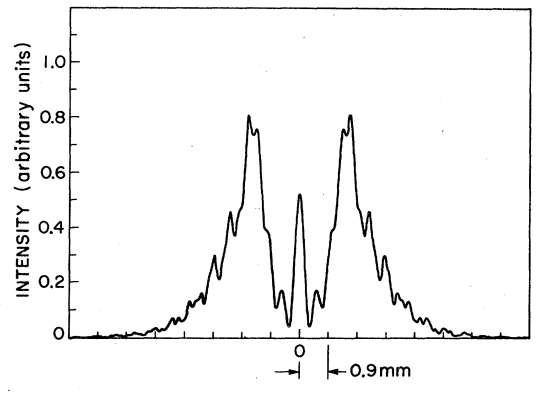

FIG. 9. The intensity profile of an unstable resonator output propagated 1 m from the laser before reaching the crystal. The resonator parameters are $M=3.5$, $N_{eq}=1.5$, and $\lambda=1.06$ μm.

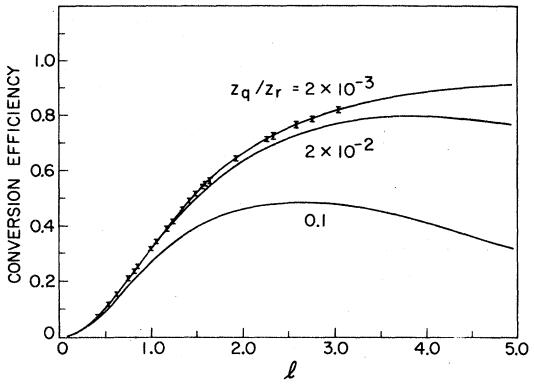

FIG. 10. The predicted and measured conversion efficiencies vs l for the fundamental beam profile shown in Fig. 9.

To measure the harmonic conversion, both the fundamental and second-harmonic pulses were displayed on a fast oscilloscope using a PIN detector. The energy in the pulses were separately measured by a thermopile and also by calibrated power meter. Since the pulse length was much longer than the dephasing time in the crystal (which is of the order of picoseconds), within the nanosecond interval the fields and the driven polarizations can be thought of as cw waves.

We digitized the intensity of the measured fundamental and harmonic waveforms at 5-nsec intervals on many different oscilloscope traces, and determined the corresponding conversion efficiencies at each point, using the measured en-

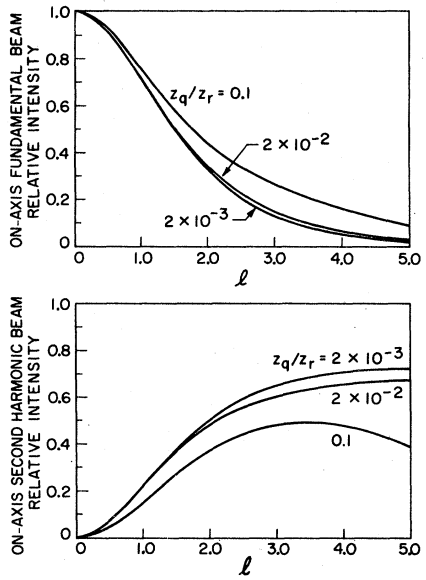

FIG. 11. Far-field on-axis relative intensity of fundamental and second-harmonic waves vs l.

ergies for normalization. The highest conversion efficiency reached was more than 80%.

The range of z_q/z_r in those experiments was within 4×10^{-4} to 3×10^{-3}, which is essentially zero so far as the theoretical curves are considered. Figure 10 shows a large number of these experimental points compared to the small z_q/z_r theoretical curve. The data fit the theoretical curve very well. Unfortunately we were not able in these experiments to reach a range of parameters which would demonstrate the turning over at large z_q/z_r and z/z_q.

Figure 11 shows the far-field on-axis intensity of both fundamental and second-harmonic waves versus normalized crystal length z/z_q. Note that the harmonic far-field intensity turns down somewhat further through the crystal than that does the total harmonic power, and the fundamental far-field intensity turns back up only very slowly if at all, as a rseult of the beam reshaping produced by the harmonic interaction.

IV. DISCUSSION

We should perhaps emphasize that we are concerned in this work with developing an approach to nonlinear wave interactions that can, at least in principle, handle real beam profiles, diffraction effects, and depletion effects completely and accurately at whatever level of complexity they may occur. If one only intends to treat simplified special cases or to handle such effects only partially or to a first order of approximation, then of course some other simplified analytical method may be much more suitable.

Results obtained using our general approach for second-harmonic generation with one-dimensional Cartesian geometry and with lowest-order ($l=0$) cylindrical symmetry have been presented in Sec. III. Other than carrying out these calculations, we have not tested our approach against any competitive approaches. Indeed it would not be easy to carry out truly competitive tests since we are not aware of other published or readily available and directly competitive numerical approaches to the same overall problem. However, we believe that our general approach should provide a technique that handles diffraction in the most effective way, through fast-transform routines, while handling the nonlinear interaction effects through efficient differential equation routines. The only alternative approach to the same class of problems of which we are aware is to use an expansion of each beam into normal modes of free space, e.g., into Hermite-Gaussian modes, and to compute coupling terms between modes.[16,17] From extensive experience with linear active laser resonator simulations using both mode-expansion and fast-transform techniques,[18,19] our conclusion is that fast-transform methods are clearly superior, at least for that purpose.

[1]J. A. Armstrong, N. Bloembergen, J. Ducuing, and P. S. Pershan, Phys. Rev. 127, 1918 (1962).
[2]D. A. Kleinman, Phys. Rev. 128, 1761 (1962).
[3]G. D. Boyd and D. A. Kleinman, J. Appl. Phys. 39, 3597 (1968).
[4]G. D. Boyd, A. Ashkin, J. M. Dziedzic, and D. A. Kleinman, Phys. Rev. 137, A1305 (1965).
[5]R. L. Herbst, H. Komine, and R. L. Byer, Opt. Commun. 21, 5 (1977).
[6]J. W. Goodman, *Introduction to Fourier Optics* (McGraw-Hill, New York, 1968).
[7]E. O. Brigham, *The Fast Fourier Transform* (Prentice-Hall, Englewood Cliffs, N. J., 1974).
[8]Lawrence R. Rabiner and Bernard Gold, *Theory and Application of Digital Signal Processing* (Prentice-Hall, Englewood Cliffs, N. J., 1975).
[9]E. A. Sziklas and A. E. Siegman, Proc. IEEE 62, 410 (1974).
[10]A. E. Siegman, Opt. Lett. 1, 3 (1977).
[11]S.-C. Sheng, Ph. D. thesis, Stanford University, 1980 (unpublished).
[12]L. F. Shampine and M. K. Gordon, *Computer Solution of Ordinary Differential Equations: The Initial Value Problem* (Freeman, San Francisco, 1975).
[13]A. Yariv, *Quantum Electronics* (Wiley, New York, 1975).
[14]A. E. Siegman, *Introduction to Lasers and Masers* (McGraw-Hill, New York, 1971), p. 318.
[15]J. E. Bjorkholm, Phys. Rev. 142, 126 (1966).
[16]R. Asby, Phys. Rev. 187, 1062 (1969).
[17]R. Asby, Phys. Rev. 187, 1070 (1969).
[18]A. E. Siegman and E. A. Sziklas, Appl. Opt. 13, 2775 (1974).
[19]E. A. Sziklas and A. E. Siegman, Appl. Opt. 14, 1874 (1975).